Article

Not peer-reviewed version

Thickness Optimization of $Zn_{0.9}Mg_{0.1}O$ Nanoparticle Electron Transport Layer for High-Performance Top-Emission Quantum Dot Light-Emitting Diodes

Gyeong-Pil Jang , Ji-Hun Yang , Su-Young. Kim , Young-Bin Chae , Hyuk-Doo Choi , Dae-Gyu Moon , Chang-Kyo Kim *

Posted Date: 1 November 2023

doi: 10.20944/preprints202311.0039.v1

Keywords: quantum dot light-emitting diode; ZnMgO nanoparticles; electro electron injection layer; charge balance; exciton quenching

Article

Thickness Optimization of $Zn_{0.9}Mg_{0.1}O$ Nanoparticle Electron Transport Layer for High-Performance Top-Emission Quantum Dot Light-Emitting Diodes

Gyeong-Pil Jang, Ji-Hun Yang, Su-Young. Kim, Young-Bin Chae, Hyuk-Doo Choi, Dae-Gyu Moon and Chang-Kyo Kim *

Department of Electronic Materials, Devices and Equipment Engineering, Soonchunhyang University, Asan, Chungnam 31538, Republic of Korea, schqled@sch.ac.kr (G.-P.J.); wlgns123789@sch.ac.kr (J.-H.Y.); swim8549@sch.ac.kr (S.-Y.K.); w200r23@sch.ac.kr (Y.-B.C.); hyukdoo.choi@sch.ac.kr, (H.-D.C.); dgmoon@sch.ac.kr (D.-G.M); ckkim1@sch.ac.kr (C.-K.Hun K.)

* Correspondence: ckkim1@sch.ac.kr; Tel.: (+82-4d1-530-1339) (C.-K.K.)

Abstract: $Zn_{0.9}Mg_{0.1}O$ nanoparticle (NP) were employed as electron transport layers (ETLs) with varying thicknesses to investigate their influence on the efficiency of the top-emission quantum dot light-emitting diodes (TE-QLEDs) fabricated inside the bank. An increase in the thickness of the $Zn_{0.9}Mg_{0.1}O$ NP ETL led to a decrease in the concentration of oxygen vacancies, reducing the conductivity of the $Zn_{0.9}Mg_{0.1}O$ and resulting in lower current density in the TE-QLEDs. The decrease in conductivity of $Zn_{0.9}Mg_{0.1}O$ NP ETL was confirmed through electron-only device (EOD) characterization. Furthermore, it was noted that when the thickness of $Zn_{0.9}Mg_{0.1}O$ NP ETL was 30 nm, the concentration of hydroxyl species reached its minimum. By minimizing the presence of hydroxyl species, exciton quenching at the quantum dot (QD) and $Zn_{0.9}Mg_{0.1}O$ NP ETL interface was minimized, enhancing charge balance within the QD, significantly improving the efficiency of QLED. We successfully demonstrated that TE-QLED with a 30 nm-thick $Zn_{0.9}Mg_{0.1}O$ NP ETL exhibits outstanding performance, achieving a maximum current efficiency of 91.92 cd/A and a maximum external quantum efficiency of 21.66%. These results suggest that $Zn_{0.9}Mg_{0.1}O$ NP ETL, when tailored to an appropriate thickness, can serve as an ETL for TE-QLEDs, effectively suppressing exciton quenching and enhancing the charge balance in the TE-QLEDs.

Keywords: quantum dot light-emitting diode; ZnMgO nanoparticles; electro electron injection layer; charge balance; exciton quenching

1. Introduction

Quantum dot (QD) light-emitting diodes (QLEDs) have emerged as highly promising contenders for next-generation display and lighting applications, boasting remarkable attributes such as exceptional color purity, tunable emission wavelength, high efficiency, and solution processability [1-6]. Due to these outstanding optoelectronic properties and advancement in device structure, QLEDs are increasingly approaching the performance of organic light-emitting diodes (OLEDs) [1-11].

One key factor influencing QLED performance is the selection and engineering of the various functional layers within the device structure. While the majority of QLEDs traditionally feature a bottom-emitting structure, there is a growing interest in top-emitting (TE) structures due to their versatility in various applications. One notable advantage of TE-QLEDs is their ability to minimize the influence of numerous integrated thin-film transistors on the substrate, which expands the range of compatible substrate materials, including opaque substrate. [13]. TE structures enable the fabrication of devices on substrates such as silicon or metal foils, thus significantly widening the possibilities for display applications.

To achieve efficient light emission, optimizing charge balance is crucial, especially in QLEDs where hole injection can be relatively inefficient when compared to electron injection. This is due to

 doi:10.20944/preprints202311.0039.v1

the higher hole injection energy barrier and disparities in electron and hole mobility [14-16]. An imbalance in hole and electron injection and transport can lead to QD charging and increase the likelihood of non-radiative Auger recombination [17-19].

ZnO nanoparticles (NPs) is widely employed as the electron transport layer (ETL) in QLEDs due to their advantages, including high mobility, transparency, and suitable interface energy level [20]. However, ZnO NPs often exhibits a significant concentration of oxygen vacancies, leading to non-radiative recombination at the QD-ZnO interface [17,21]. When the QD emission layer (EML) is in direct contact with ZnO NP ETL, spontaneous electron transfer occurs at the interface, resulting in exciton quenching [22,23]. Excitons in QD EML are susceptible to quenching through interfacial charge transfer processes and/or intragap-assisted non-radiative recombination centers [18]. Consequently, addressing the interface between the QD EML and ZnO NP ETL is crucial to enhance device performance. One approach to alleviate exciton quenching is to insert an insulating layer between the QD EML and ZnO NP ETL. Zhang et al. reported a red QLED with a low turn-on voltage of 1.7 V, a high peak external quantum efficiency (EQE) of 20.5%, and a long lifetime of over 1,000,000 h at an initial brightness of 100 cd/m^2 [24]. The enhanced performance is attributed to the poly(methyl methacrylate) (PMMA) insulating layer placed between the QD EML and ZnO NP ETL, effectively preventing the exciton quenching.

Another approach to mitigate this issue is the introduction of magnesium (Mg) into ZnO NPs (ZnMgO), which has been shown to reduce the concentration of oxygen vacancies in ZnO NPs [24]. These modifications are believed to reduce exciton quenching and enhance efficiency in QLEDs. As a result, extensive study has focused on optimizing Mg doping in ZnO NPs, resulting in changes in energy bandgap and modifications in conductivity attributed to variations in the concentration of oxygen vacancies [19,24-26]. Chrzanowski et al. developed QLEDs by adjusting the Mg content in the ZnMgO NP ETL, ranging from 0% to 20%. The QLED with a ZnMgO NP ETL containing 15% Mg demonstrated a maximum current efficiency of 18 cd/A and a maximum EQE of 5.74% [27]. Moon et al. conducted experiments using ZnMgO NPs with tailored Mg composition as the ETLs for InP-based QLEDs. They achieved their highest maximum luminance of 13,000 cd/ m^2 and an EQE of 13.6% when the Mg content was 12.5 mol% [28]. Kim et al. reported Cu-In-S/ZnS-based QLEDs by varying the Mg content in the ZnMgO NP ETL from 0% to 10%. Notably, the QLED with a ZnMgO NP ETL containing 10% Mg exhibited a maximum current efficiency of 5.75 cd/A [29]. Meanwhile, Heo et al. demonstrated QLEDs using ZnMgO as an interfacial layer between the QD EML and ZnO NP ETL. This approach resulted in an impressive 86.9% increase in EQE, achieved through a stepwise interfacial electronic structure and effectively blocked direct contact between the QD EML and ZnO NP ETL [19]. In a similar vein, Wang et al. also reported QLEDs that incorporated the ZnMgO layer between the QD EML and ZnO NP EML. This configuration reduced electron injection from ZnO ETL into QD EML and successfully suppressed exciton quenching at the interface of QD EML and ZnMgO NP ETL. As a result, the maximum current efficiency improved from 2.31 cd/A for a red QLED with only a ZnO ETL to 5.48 cd/A for a red QLED with the inclusion of the ZnMgO layer between the QD EML and ZnO NP ETL [25]. Sun et al. also reported inverted red QLEDs with a ZnMgO/ZnO double ETL, which reduces the electron injection, improves the balance of charge injection, and significantly mitigates the exciton quenching by ZnO NPs, where ZnMgO was used as an interfacial layer. The red QLED with a ZnMgO/ZnO double ETL exhibits a maximum current efficiency of 18.69 cd/A, representing a 71.8% enhancement in maximum current efficiency when compared to the red QLED with only a ZnO ETL [26]. Qu et al., reported that there is no exciton quenching at the interface of the QD EML and ZnMgO NP ETL if the film is well encapsulated [26]. Zhang et al. further demonstrates QLEDs by varying the thickness of the ZnMgO NP ETL, ranging from 60 nm to 165 nm. The QLED with a 110-nm-thick ZnMgO NP ETL exhibited a peak EQE of 17.0%. Moreover, several groups have developed high-efficiency QLEDs by employing a core-shell structure with ZnMgO as the ETL to passivate defects in ZnO NPs, thereby increasing the Mg concentration in the shell layer [30-32]. Rather than focusing on direct contact between QDs and ZnO NPs, extensive study is currently underway regarding direct contact between QDs and ZnMgO NPs.

 doi:10.20944/preprints202311.0039.v1

This paper presents the development of highly efficient TE-QLEDs achieved by adjusting the thickness of the ZnMgO NP ETL, resulting in modifications that include variations in conductivity due to changes in oxygen vacancy concentration, and alterations in quenching sites influenced by changes in hydroxyl (-OH) species concentration. By employing X-ray photoelectron spectroscopy (XPS) measurement, the study examined the concentration of oxygen vacancy and the concentration of hydroxyl species. This analysis aimed to understand electron injection and electron transport mechanism in the ZnMgO ETL, as well as non-radiation recombination at the QD-ZnMgO interface. As a result, the presented TE-QLED with a 30-nm-thick $Zn_{0.9}Mg_{0.1}O$ NP ETL demonstrated outstanding performance, achieving a maximum current efficiency of 91.92 cd/A and a maximum EQE of 21.66%. We believe that employing $Zn_{0.9}Mg_{0.1}O$ NP ETL with an appropriate thickness holds promise for achieving high-performance TE-QLEDs suitable for next-generation displays and lighting applications.

2. Materials and Methods

2.1. Synthesis of Materials

For the synthesis of $Zn_{0.9}Mg_{0.1}O$ NPs [30], we commenced by dissolving 0.2962 g of zinc acetate dihydrate ($Zn(CH_3COO)\cdot 2H_2O$) powder (Sigma-Aldrich) and 0.03292 g of magnesium acetate tetrahydrate ($Mg(CH_3COO)\cdot 4H_2O$) powder (Sigma-Aldrich), which served as precursor materials, in 15 mL of dimethyl sulfoxide (DMSO). Additionally, 0.421 g of TMAH (Sigma Aldrich) were dissolved in 5 mL of EtOH. The TMAH solution was then blended with the solution containing $Zn(CH_3COO)\cdot 2H_2O$ and $2Mg(CH_3COO)\cdot 4H_2O$), and the mixture was stirred at room temperature for 24 h to ensure complete dissolution. Subsequently, we introduced ethyl acetate (Kanto Chemical Co.) into the synthesized solution to precipitate the $Zn_{0.9}Mg_{0.1}O$ NPs, using a volume ratio of 3:1 for ethyl acetate to the synthesized solution. After 3 h, a white powder had formed and precipitated. $Zn_{0.9}Mg_{0.1}O$ NPs were obtained through centrifugation.

2.2. Device Fabrication

TE-QLEDs were fabricated by a solution-process approach. A glass substrate underwent a rigorous cleaning process involving acetone, isopropyl, alcohol, methanol, and deionized water. Following the cleaning process, the substrate was subjected to treatment with oxygen plasma.

A solution of poly (3,4-ethylenedioxythiophene):poly (styrene sulfonate) (PEDOT:PSS) (Al4083; Heraeus) dissolved in isopropanol (Daejung Co., Ltd.) was applied onto a glass substrate using a spin-coating method. Following this, the PEDOT:PSS film underwent a baking process at 60°C for 10 m in an air environment to eliminate any residual water within the film. The resulting PEDOT:PSS film had a thickness of 25 nm. PEDOT:PSS was selected as a buffer layer, positioned between the glass substrate and the Ag anode to enhance adhesion during the Ag evaporation process onto the glass substrate and improve the electrical conductivity of Ag anode. Subsequently, the glass substrates with PEDOT:PSS buffer layer were placed inside a high-vacuum deposition chamber (Cetus OL 100; Celcose, Hwasung, Korea) with a background pressure, 6×10^{-7} Torr. Within this chamber, a 150-nm-thick Ag anode layer was deposited at an evaporation rate of 1.2 Å/s. The anode layer was patterned using an *in-situ* shadow mask to form the desired anode pattern.

A bank layer was fabricated onto the Ag anode to eliminate the leakage current between anode and cathode the photolithography method. SU-8 (SU-8 2002, Kayaku Advanced Materials) was deposited onto Glass/PEDOT:PSS/Ag substrate by spin-coating at a speed of 500 rpm for 5 s at room temperature, followed by spin-coating at a speed of 3,000 rpm for 30 s at room temperature. The formed SU-8 thin film was subjected to a soft bake at 90℃ on hot plate for 2 min to evaporate the solvent and create the thin film. The substrate with the formed SU-8 thin film was aligned with the mask of the bank layer pattern on the Mask Aligner (ABM, ABM/6/350/NUV/DDD/M) and exposed to UV light at a wavelength of 365 nm for 15.6 s. The UV-exposed SU-8 underwent polymerization and crosslinking, rendering it insoluble. After UV exposure, a post exposure bake was performed at

 doi:10.20944/preprints202311.0039.v1

95℃ on a hot plate for 2 min. The UV-exposed SU-8 is developed in an SU-8 developer for 1 min to remove the unexposed portions, followed by a 10 s rinse in isopropyl alcohol (IPA) (Daejung Chemicals and Metals, Gyeonggi, Republic of Korea) for cleaning. Nitrogen was then used to remove moisture. Lastly, any remaining developer or cleaning solution was removed during development, and to enhance adhesion, a hard bake is conducted on a 150℃ hot plate for 30 m to complete the bank layer.

To serve as an HIL, additional layer of PEDOT:PSS layer was spin-coated onto the Glass/PEDOT:PSS/Ag substrate inside the bank using the same method as described earlier. For use as an HTL, a solution of poly(9 vinylcarbazole) (PVK) solution dissolved in toluene was coated onto the pre-fabricated Glass/PEDOT:PSS/Ag/PEDOT:PSS substrate inside the bank. The PVK film was annealed in air at 60℃ for 10 min. The resulting PVK film had a thickness of 40 nm. To fabricate the QD EML, CdSe/ZnS QDs (Zeus) were dissolved at concentration of 5 mg/mL in heptane. This solution was then spin-coated onto the Glass/PEDOT:PSS/Ag/PEDOT:PSS/PVK substrate inside the band. The QD film had a thickness of 10 nm. ZnMgO NP solution was spin-coated onto the Glass/PEDOT:PSS/Ag/PEDOT:PSS/PVK/QD substrate inside the bank. Finally, 15-nm-thick Ag used as a cathode was deposited onto the Glass/PEDOT:PSS/Ag/PEDOT:PSS/PVK/QD/ZnMgO NPs substrate inside the bank using the same method employed for depositing the Ag electrode used as the anode to complete TE-QLEDs. Figure 1 illustrates a schematic diagram of the TE-QLED configuration.

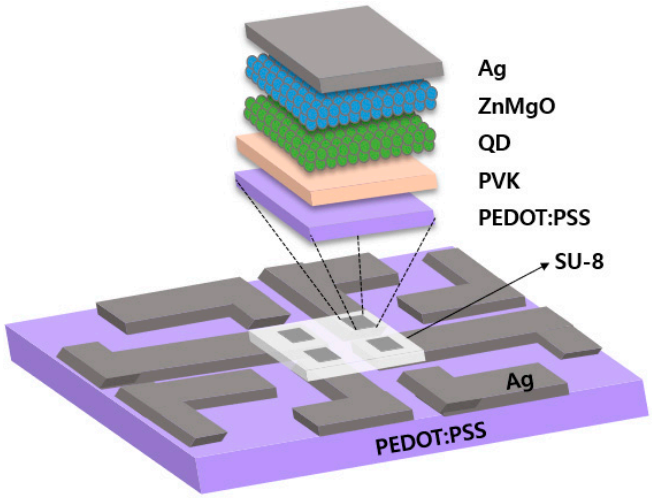

Figure 1. Schematic diagram of the TE-QLED configuration.

2.3. Characterizations

To examine the crystal structure of ZnMgO NPs, X-ray diffraction (XRD: D/Max-2200pc; Rigaku, Tokyo, Japan) patterns were obtained using Cu-Kα radiation applied to the centrifuged ZnMgO NPs. Field-emission transmission electron microscopy (FE-TEM) (Tecnai F30 S-Twin; JEOL Ltd., Tokyo, Japan) was employed to determine the actual particle size of the ZnMgO NPs. X-ray photoelectron spectroscopy (XPS) was conducted using ThermoFisher Scientific, Waltham, MA, USA to investigate the composition of ZnMgO NP films and UPS analysis, employing a He (I) 21.22-eV gas discharge lamp, was performed to characterize the electronic structure of the ZnMgO NPs based ETL thin films. Transmittance and reflectance measurements were conducted using a spectrophotometer (UV-1650PC; Shimadzu Corp., Kyoto, Japan), with normally incident monochromatic light at the sample surface side. Current density–voltage–luminance (*J*–*V*–*L*) characteristics were evaluated using a computer-controlled source meter (2400; Keithley Instruments, Cleveland, OH, USA) in conjunction with a luminance meter (LS100; Konica Minolta, Tokyo, Japan). Electroluminescence (EL) spectra were recorded using a spectroradiometer (CS1000; Konica Minolta).

Preprints (www.preprints.org) | NOT PEER-REVIEWED | Posted: 1 November 2023 doi:10.20944/preprints202311.0039.v1

3. Results and Discussion

Figure 2 illustrates the characteristic X-ray diffraction (XRD) pattern of the $Zn_{0.9}Mg_{0.1}O$ NPs obtained by scanning the 2θ range. The XRD pattern was analyzed to investigate the crystal structure and crystallite size of $Zn_{0.9}Mg_{0.1}O$ NPs. It reveals a hexagonal wurtzite structure, which is characteristic feature of ZnO, as confirmed by comparing it to the Joint Committee on Powder Diffraction Standards (JCPDS Card No. 1-1136). The XRD pattern of $Zn_{0.9}Mg_{0.1}O$ NPs exhibits reflections in the (100), (002), (101), (102), (110), (103) and (112) planes, all of which are attributable to the ZnO phase. A slight shift in the diffraction peak and intensity of the $Zn_{0.9}Mg_{0.1}O$ NPs is observed, suggesting a minor lattice distortion and altered interatomic spacing.

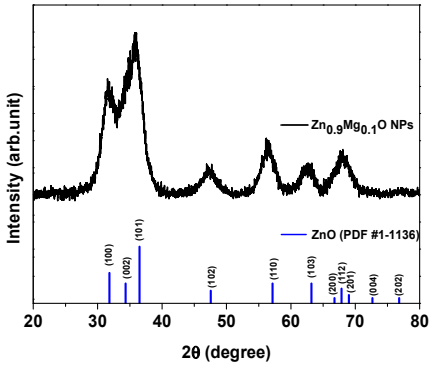

Figure 2. X-ray diffraction pattern of $Zn_{0.9}Mg_{0.1}O$ nanoparticles (NPs) over a 2θ scanning range of 20-80°.

Figure 3 presents a typical field-emission transmission electron microscopy (FE-TEM) image of the $Zn_{0.9}Mg_{0.1}O$ NPs. The size of the $Zn_{0.9}Mg_{0.1}O$ NPs was determined through FE-TEM analysis, revealing an average diameter of 4.61 nm.

XPS measurements were conducted to examine the oxygen configuration of $Zn_{0.9}Mg_{0.1}O$ NP thin film as a function of varying thickness, providing information about the quality of the NPs, as shown in Figure 4. This figure illustrates the normalized O 1s spectra of the $Zn_{0.9}Mg_{0.1}O$ NPs deposited onto the PEDOT:PSS (25 nm)/Ag (150 nm)/PEDOT:PSS (25 nm)/QD (10 nm) substrate. By employing deconvolution, three peaks were extracted, each corresponding to specific components, including the metal oxide lattice bond (O_M), oxygen vacancies O^{2-} ions (O_V), and hydroxyl (O_{OH}) species. [33]. The area of each peak exhibited variations depending on the thickness of the $Zn_{0.9}Mg_{0.1}O$ NP thin film [34-36]. O_T represents the overall O 1s peak. Figure 4(e) includes a distribution graph illustrating the ratio of the areas of the three peaks areas concerning the thickness of $Zn_{0.9}Mg_{0.1}O$ NP thin film. The ratios of the peak area (O_V/O_T) of 10-nm-thick $Zn_{0.9}Mg_{0.1}O$ NP thin film, 30-nm-thick $Zn_{0.9}Mg_{0.1}O$ NP thin film, 50-nm-thick $Zn_{0.9}Mg_{0.1}O$ NP thin film, and 70-nm-thick $Zn_{0.9}Mg_{0.1}O$ NP thin film were calculated to be 35.46%, 27.20%, 25.26%, and 21.70%, respectively. On the other hand, the ratios of the peak area (O_{OH}/O_T) of 10-nm-thick $Zn_{0.9}Mg_{0.1}O$ NP thin film, 30-nm-thick $Zn_{0.9}Mg_{0.1}O$ NP thin film, 50-nm-thick $Zn_{0.9}Mg_{0.1}O$ NP thin film, and 70-nm-thick $Zn_{0.9}Mg_{0.1}O$ NP thin film were estimated to be 9.36%, 0.57%, 3.67%, and 5.10%, respectively. With an increase in thickness, there was a noticeable trend towards a higher concentration of metal oxide lattice bonds, while the concentration of the oxygen vacancies decreased. The oxygen vacancies act as trap sites, and an increase in these sites leads to higher carrier concentration, enhanced conductivity, and reduced resistance of the $Zn_{0.9}Mg_{0.1}O$ NP thin film [37]. Furthermore, the XPS results indicate that the $Zn_{0.9}Mg_{0.1}O$ NP thin film with a thickness of 30 nm exhibits the lowest concentration of hydroxyl species. A reduction in the hydroxyl species within the $Zn_{0.9}Mg_{0.1}O$ NP thin film resulted in reduced quenching effects at interface, thereby extending the lifetime of QDs [38]. Based on these results, it can be expected that TE-QLEDs with a 30-nm-thick $Zn_{0.9}Mg_{0.1}O$ NP ETL will demonstrate high luminance and EQE.

Preprints (www.preprints.org) | NOT PEER-REVIEWED | Posted: 1 November 2023 doi:10.20944/preprints202311.0039.v1

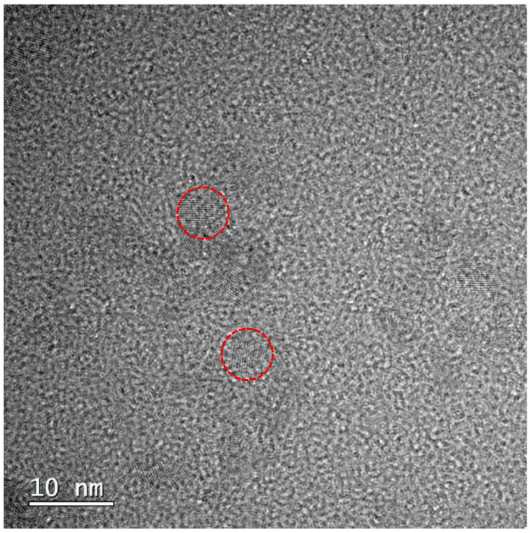

Figure 3. Field-emission transmission electron microscopy of $Zn_{0.9}Mg_{0.1}O$ NPs.

To investigate the influence of the bank enclosure on leakage current, electroluminescent characteristics were examined. Figure S1(a) depicts the current density versus applied voltage curves of TE-QLED with a 50-nm-thick $Zn_{0.9}Mg_{0.1}O$ NP ETL with a 50-nm-thick $Zn_{0.9}Mg_{0.1}O$ NP ETL, both fabricated inside and without the bank enclosure. It is noteworthy that when voltages of up to 8 V were applied, the TE-QLED with a 50-nm-thick $Zn_{0.9}Mg_{0.1}O$ NP ETL fabricated without the bank enclosure exhibited a higher leakage current, characterized by a raised, and rounded peak. In contrast, the TE-QLED with a 50-nm-thick $Zn_{0.9}Mg_{0.1}O$ NP ETL fabricated inside the bank enclosure did not exhibit such a raised and rounded peak and had a much lower leakage current. Additionally, throughout the entire measurement range, the current density of the TE-QLED with a 50-nm-thick $Zn_{0.9}Mg_{0.1}O$ NP ETL fabricated without the bank enclosure was higher than that of the TE-QLED with a 50-nm-thick $Zn_{0.9}Mg_{0.1}O$ NP ETL fabricated inside the bank enclosure, likely due to leakage current.

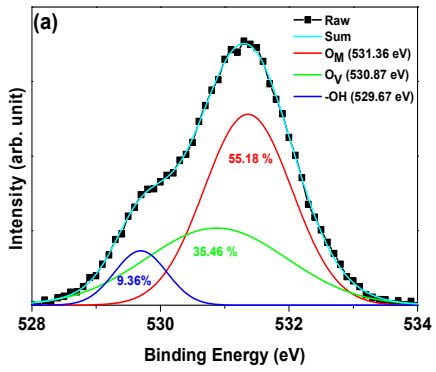

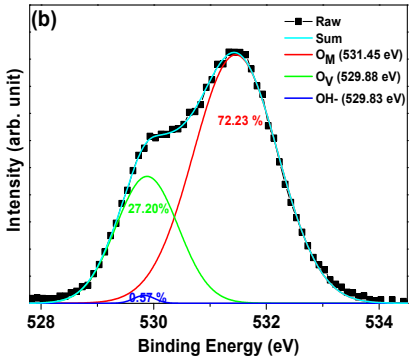

Preprints (www.preprints.org) | NOT PEER-REVIEWED | Posted: 1 November 2023 doi:10.20944/preprints202311.0039.v1

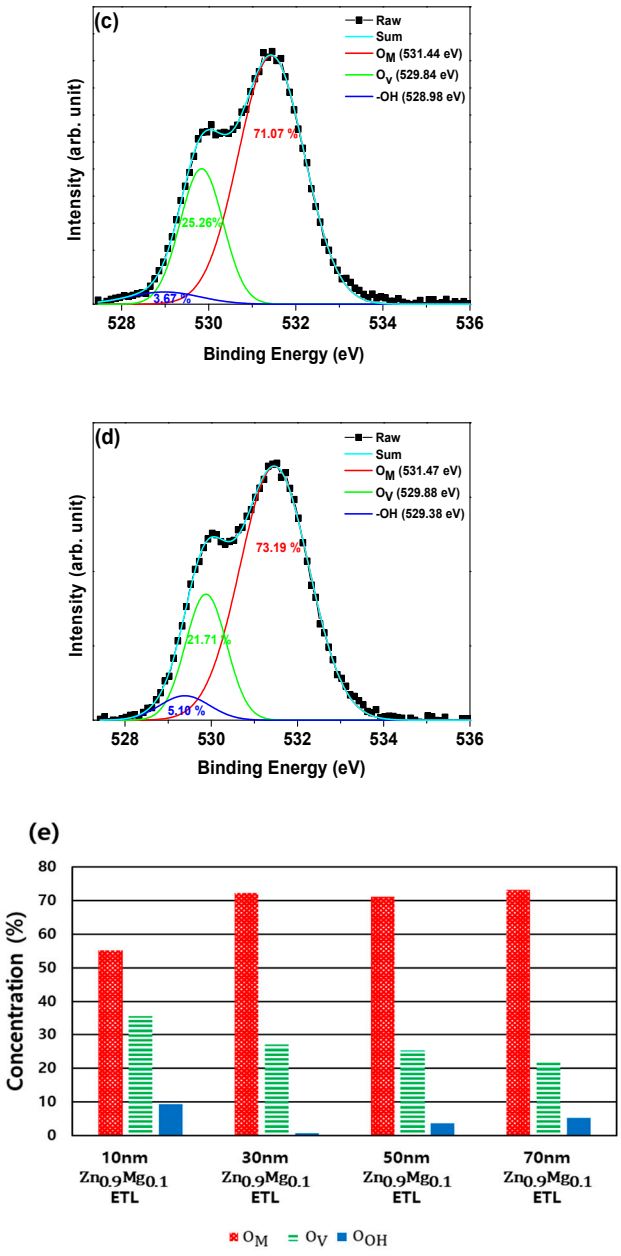

Figure 4. X-ray photoelectron spectroscopy O 1s spectra of $Zn_{0.9}Mg_{0.1}O$ NP thin films with varying thickness deposited onto a PEDOT:PSS/Ag/PEDOT:PSS/PVK/QD substrate: (a) 10-nm-thick $Zn_{0.9}Mg_{0.1}O$ NP thin films, (b) 30-nm-thick $Zn_{0.9}Mg_{0.1}O$ NP thin films, (c) 50-nm-thick $Zn_{0.9}Mg_{0.1}O$ NP thin films, (d) 70-nm-thick $Zn_{0.9}Mg_{0.1}O$ NP thin films. (e) Area ratio of each of the three peaks in relation to the change in thickness of $Zn_{0.9}Mg_{0.1}O$ NP thin films. .

Figure S1(b) illustrates that the turn-on volage at 1 cd/m² of the TE-QLED with a 50-nm-thick $Zn_{0.9}Mg_{0.1}O$ NP ETL fabricated inside the bank enclosure was lower than that of the TE-QLED with a 50-nm-thick $Zn_{0.9}Mg_{0.1}O$ NP ETL fabricated without the bank enclosure. Additionally, in the low voltage range, the TE-QLED with a 50-nm-thick $Zn_{0.9}Mg_{0.1}O$ NP ETL fabricated inside the bank enclosure exhibited higher luminance compared to the TE-QLED with a 50-nm-thick $Zn_{0.9}Mg_{0.1}O$ NP ETL fabricated without the bank enclosure. This suggests that the charge balance between electrons and holes within the EML of the TE-QLED with a 50-nm-thick $Zn_{0.9}Mg_{0.1}O$ NP ETL fabricated inside the bank enclosure was better achieved in the low voltage range. However, in the high voltage range, the TE-QLED with a 50-nm-thick $Zn_{0.9}Mg_{0.1}O$ NP ETL fabricated inside the bank enclosure exhibited lower luminance than the TE-QLED with a 50-nm-thick $Zn_{0.9}Mg_{0.1}O$ NP ETL fabricated without the

Preprints (www.preprints.org) | NOT PEER-REVIEWED | Posted: 1 November 2023 doi:10.20944/preprints202311.0039.v1

bank enclosure. This indicates that in the high voltage range, the charge balance between electrons and holes within the EML of the TE-QLED with a 50-nm-thick $Zn_{0.9}Mg_{0.1}O$ NP ETL fabricated inside the bank was not as effectively achieved as in the counterpart without bank enclosure, leading to an observed roll-off in the current efficiency in the TE-QLED with a 50-nm-thick $Zn_{0.9}Mg_{0.1}O$ NP ETL fabricated inside the bank enclosure.

Figure S1(c) presents the current efficiency versus applied voltage curves of TE-QLEDs with a 50-nm-thick $Zn_{0.9}Mg_{0.1}O$ NP ETL, both fabricated inside and without the bank enclosure. It is evident that the TE-QLED with a 50-nm-thick $Zn_{0.9}Mg_{0.1}O$ NP ETL fabricated inside the bank enclosure achieved a higher maximum current efficiency compared to its counterpart fabricated without the bank enclosure. This improvement can be attributed to the bank enclosure's role in constraining leakage current.

Figure S1(d) illustrates the electroluminescence (EL) spectra of the TE-QLEDs with a 50-nm-thick $Zn_{0.9}Mg_{0.1}O$ NP ETL, both fabricated inside and without the bank enclosure. Both TE-QLEDs have their peak values centered at 524 nm. However, the full width at half maximum (FWHM) of the TE-QLED fabricated inside the bank enclosure is narrower than that of the TE-QLED fabricated without the bank enclosure. This indicates that the charge balance in the EML of the TE-QLED fabricated inside the bank enclosure is better achieved than in the TE-QLED fabricated without the bank.

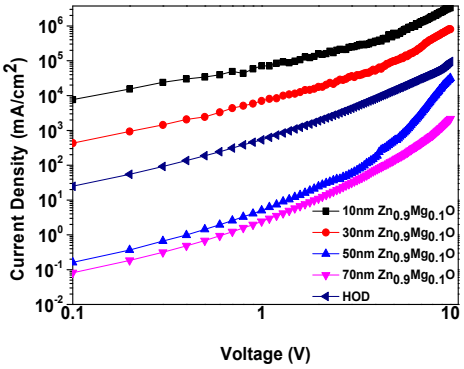

Figure 5. Current density versus applied voltage of the electron-only devices (EODs) according to various thickness of $Zn_{0.9}Mg_{0.1}O$ NPs (10 nm, 30 nm, 50 nm, and 70 nm), and the hole-only device (HOD).

Electron-only devices (EODs) and hole-only devices (HOD) were fabricated to investigate the hole and electron injection, as well as electron transport behaviors. Four different EODs were developed, each with varying $Zn_{0.9}Mg_{0.1}O$ NPs thickness (10 nm, 30 nm, 50 nm, and 70 nm), as illustrated in Figure 6. Additionally, a HOD was also created. The EOD structures consisted of Ag (150 nm)/$Zn_{0.9}Mg_{0.1}O$ NPs (10 nm, 30 nm, 50 nm, 70 nm)/QD (10 nm)/$Zn_{0.9}Mg_{0.1}O$ NPs (10 nm, 30 nm, 50 nm, 70 nm)/Ag (150 nm), while the HOD structure was Ag (150 nm)/PEDOT:PSS (25 nm)//PVK (40 nm)/QD (10 nm)/Ag (150 nm). The thickness of the $Zn_{0.9}Mg_{0.1}O$ NPs on both sides of the QDs for EODs was the same. The additional layer of $Zn_{0.9}Mg_{0.1}O$ NPs on the anode side was added to block incoming holes from the anode and prevent excessive current flow through the device. Electrons can be injected from the cathode to the conduction band minimum (CBM) level of QDs via the CBM level of ZnMgO NPs. The measurements from EODs revealed that as the thickness of the $Zn_{0.9}Mg_{0.1}O$ NPs increased, the current density of EODs decreased. This observation is consistent with the XPS results, which show a reduction in oxygen vacancy as the thickness of $Zn_{0.9}Mg_{0.1}O$ NPs increases. This leads to decreased conductivity and an increase in resistance of the $Zn_{0.9}Mg_{0.1}O$ NP ETL. Furthermore, an increase in thickness of the $Zn_{0.9}Mg_{0.1}O$ NP ETL leads to higher resistance. The current density obtained from HOD fell within the range of the current densities obtained from EODs with thickness of 30 nm and 50 nm. This implies that optimal charge balance in the QD EML can be achieved in the TE-QLED when using either a 30 nm or 50 nm thickness of ZnMgO as the ETL.

Preprints (www.preprints.org) | NOT PEER-REVIEWED | Posted: 1 November 2023 doi:10.20944/preprints202311.0039.v1

Figure 6 illustrates the EL characteristics of the TE-QLEDs employing $Zn_{0.9}Mg_{0.1}O$ NP ETLs with varying thicknesses: 10 nm, 30 nm, 50 nm, and 70 nm. In Figure 6(a), the curves for current density and luminance are presented as functions of applied voltage. It is noteworthy that as the thickness of the $Zn_{0.9}Mg_{0.1}O$ NP ETL increases, there is a notable decrease in current density. This phenomenon can be attributed to a reduction in conductivity resulting from a decreased concentration of oxygen vacancies within the $Zn_{0.9}Mg_{0.1}O$ NP ETL, as supported by XPS results. Furthermore, this decrease in current density can also be linked to the decreased electric field, resulting from the increased thickness of the ETL.

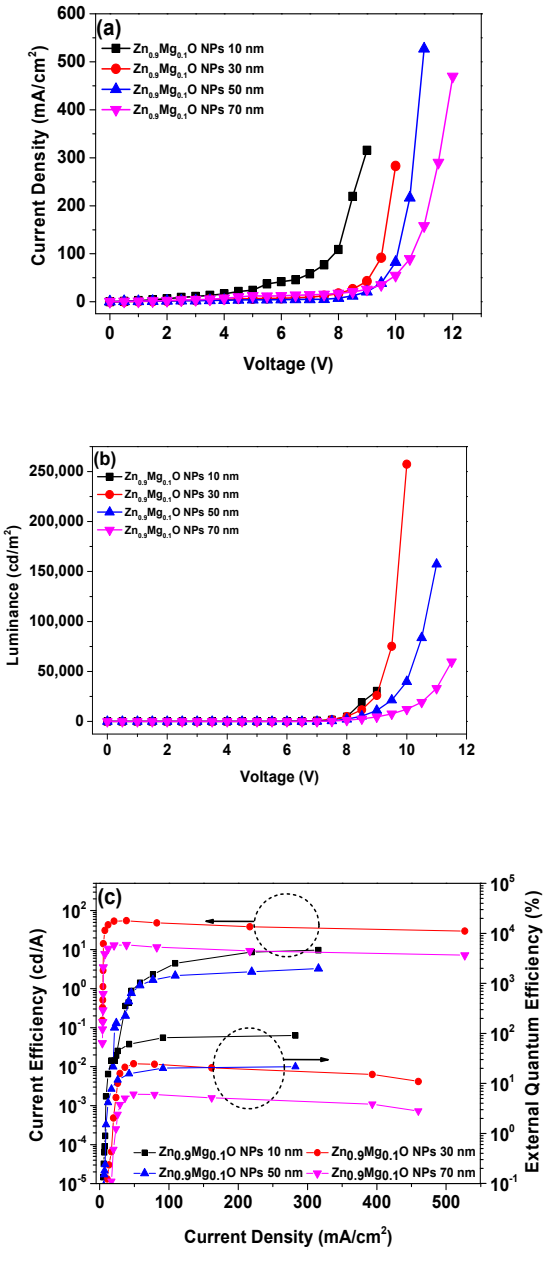

Figure 6. Electroluminescence (EL) characteristics of the TE-QLEDs utilizing $Zn_{0.9}Mg_{0.1}O$ NP ETLs with different thicknesses: 10 nm, 30 nm, 50 nm, and 70 nm: (a) Current density-voltage curves as a function of voltage, (b) luminance curves as a function of current density, and (c) current efficiency and external quantum efficiency curves as a function of current efficiency. .

The turn-on voltages at 1 cd/m² for the TE-QLEDs with 10-nm-thick, 30-nm-thick, 50-nm-thick, and 70-nm-thick $Zn_{0.9}Mg_{0.1}O$ NP ETLs were extrapolated to be 4.15 V, 4.06 V, 4.57 V, 4.65 V, and 4.52 V, respectively. This indicates that the TE-QLED with a 30-nm-thick $Zn_{0.9}Mg_{0.1}O$ NP ETL exhibited

Preprints (www.preprints.org) | NOT PEER-REVIEWED | Posted: 1 November 2023 doi:10.20944/preprints202311.0039.v1

the lowest turn-on voltage, indicating minimized exciton quenching at the interface between the QD and $Zn_{0.9}Mg_{0.1}O$ NP ETL. This reduction can be attributed to a decrease in hydroxyl species, as confirmed by XPS analysis, and the achievement of optimal charge balance in the QD EML. Additionally, Figure 6(a) illustrates the maximum luminance values of TE-QLEDs with 10-nm-thick, 30-nm-thick, 50-nm-thick, and 70-nm-thick $Zn_{0.9}Mg_{0.1}O$ NP ETLs, estimated at 30,560.1 cd/m², 257,307.4 cd/m², 157,337.4 cd/m², and 59,782.06 cd/m², respectively. The TE-QLED with a 30-nm-thick ZnMgO NP ETL exhibited the highest luminance among the four TE-QLEDs with varying $Zn_{0.9}Mg_{0.1}O$ NP ETL thicknesses. This observation was confirmed by analysis of EODs and HOD, as shown in Figure 3, suggesting that a balanced charge distribution between electrons and holes within the QD EML was likely more effectively achieved in the TE-QLED with a 30-nm-thick ZnMgO NP ETL or the one with a 50-nm-thick ZnMgO NP ETL. Moreover, it is believed that the lower concentration of hydroxyl species in the ZnMgO NPs, as observed in the XPS analysis depicted in Figure 4, minimized exciton quenching at the interface between QD EML and $Zn_{0.9}Mg_{0.1}O$ NP ETL, resulting in higher luminance.

Figure 6(c) presents the current efficiencies and EQE of the TE-QLEDs employing $Zn_{0.9}Mg_{0.1}O$ NP ETLs with different thicknesses: 10 nm, 30 nm, 50 nm, and 70 nm. The maximum current efficiencies of TE-QLEDs with 10-nm-thick, 30-nm-thick, 50-nm-thick, and 70-nm-thick $Zn_{0.9}Mg_{0.1}O$ NP ETLs were measured at be 9.68 cd/A, 90.92 cd/A, 55.33 cd/A, and 20.98 cd/A, respectively. Simultaneously, the maximum EQEs for TE-QLEDs with 10-nm-thick, 30-nm-thick, 50-nm-thick, and 70-nm-thick $Zn_{0.9}Mg_{0.1}O$ NP ETLs were estimated to be 3.28%, 21.66%, 13.22%, and 6.08%, respectively. Remarkably, the TE-QLED with a 30-nm-thick $Zn_{0.9}Mg_{0.1}O$ NP ETL exhibited an outstanding maximum current efficiency and maximum EQE of 90.92 cd/A and 21.66%, respectively. These results align with our earlier discussion, underscoring the significance of choosing the right $Zn_{0.9}Mg_{0.1}O$ NP ETL thickness to achieve charge balance and minimize the concentration of hydroxyl species acting as quenching sites at the interface between QD EML and $Zn_{0.9}Mg_{0.1}O$ NP ETL at that thickness. Table 1 summarizes the key parameters obtained from the TE-QLEDs employing $Zn_{0.9}Mg_{0.1}O$ NP ETLs with varying thicknesses: 10 nm, 30 nm, 50 nm, and 70 nm.

Figure 7 illustrates the normalized photoluminescence (PL) spectrum of the CdSe/ZnS QD, along with EL spectra from the TE-QLEDs employing $Zn_{0.9}Mg_{0.1}O$ NP ETLs with various thicknesses: 10 nm, 30 nm, 50 nm, and 70 nm. A summary of the characteristic parameters for these spectra is provided in Table 2. The EL peak of the TE-QLED with a 10-nm-thick $Zn_{0.9}Mg_{0.1}O$ NP ETL is centered at 524 nm, matching the PL peak of the CdSe/ZnS QD. In contrast, the EL peaks of TE-QLEDs with 30-nm thick, 50-nm-thick, and 70-nm-thick $Zn_{0.9}Mg_{0.1}O$ NP ETLs are centered at 532 nm, indicating a red-shift compared to the PL peak of the CdSe/ZnS QD. These red shifts can be attributed to factors such as Föster energy transfer, dielectric dispersions, and the Stark effect occurring under high voltage and current conditions [39,40]. Furthermore, Figure 8 also demonstrates that the spectra's FWHM increases as the thickness of the $Zn_{0.9}Mg_{0.1}O$ NP ETLs increases. However, when the thickness of the $Zn_{0.9}Mg_{0.1}O$ NP ETL is 10 nm, it is considered too thin to have a significant impact. The TE-QLED with a 30-nm-thick $Zn_{0.9}Mg_{0.1}O$ NP ETL exhibited the narrowest FWHM of 328 nm, indicating that the best charge balance occurred in the QD EML. The absence of parasitic PVK emission confirms that the device emission primarily results from electron-hole recombination within the CdSe/ZnS QD EML. These findings can be attributed to the effective charge balance achieved between holes and electrons within the e CdSe/ZnS QD EML

Table 1. The performance parameters of TE-QLEDs with various thickness of $Zn_{0.9}Mg_{0.1}O$ NPs.

Thickness of $Zn_{0.9}Mg_{0.1}O$ NP ETL (nm)	Turn-on voltage at Current Density (V)	Turn-on voltage at 1 cd/m² (V)	Current Density at 9 V (mA/cm²)	Maximum Luminance (cd/m²)	Maximum Current Efficiency (cd/A)	Maximum EQE (%)
10	0.49	4.15	315.75	30560.06	9.68	3.28
30	1.51	4.06	42.75	257307.4	90.92	21.66

Preprints (www.preprints.org) | NOT PEER-REVIEWED | Posted: 1 November 2023 doi:10.20944/preprints202311.0039.v1

50	0.99	4.57	20.75	157337.4	55.33	13.22
70	0.99	4.65	25.75	59782.06	20.98	6.08

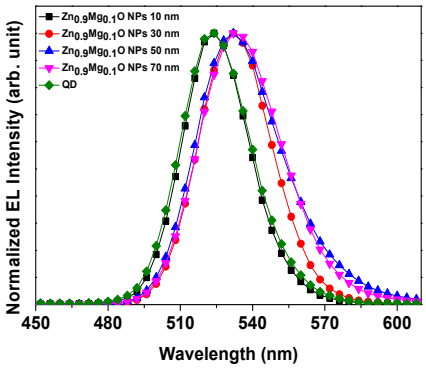

Figure 7. Normaized photoluminescence spectrum of the CdSe/ZnS quantum dot (QD) and EL spectra of the TE-QLEDs utilizing $Zn_{0.9}Mg_{0.1}O$ NP ETLs with different thicknesses: 10 nm, 30 nm, 50 nm, and 70 nm.

Table 2. Normalized photoluminescence (PL) spectrum of the CdSe/ZnS QD and electroluminescence (EL) spectra of the TE-QLEDs with various thickness of $Zn_{0.9}Mg_{0.1}O$ NPs.

Sample	Peak (nm)	FWHM (nm)
PL of QD	524	33.8
EL of TE-QLED with 10 nm $Zn_{0.9}Mg_{0.1}O$ NP ETL	524	32.8
EL of TE-QLED with 30 nm $Zn_{0.9}Mg_{0.1}O$ NP ETL	532	35.5
EL of TE-QLED with 50 nm $Zn_{0.9}Mg_{0.1}O$ NP ETL	532	40.4
EL of TE-QLED with 70 nm $Zn_{0.9}Mg_{0.1}O$ NP ETL	532	41.9

4. Conclusions

$Zn_{0.9}Mg_{0.1}O$ NP ETLs with varying thickness were synthesized to investigate their influence on the efficiency of the TE-QLEDs. These TE-QLEDs, each $Zn_{0.9}Mg_{0.1}O$ NP ETL with different thicknesses, were fabricated inside the SU-8 bank enclosure. The bank enclosure was fabricated on a PEDOT:PSS/Ag anode substrate, and the TE-QLEDs were subsequently prepared on the PEDOT:PSS/Ag anode inside the bank enclosure. The bank enclosure effectively boosted the maximum current efficiency by constraining any leakage current between the Ag anode and Ag cathode. XPS measurements were employed to examine the concentrations of oxygen vacancy and hydroxyl species in relation to the varying thickness of $Zn_{0.9}Mg_{0.1}O$ NP ETLs. As the thickness increased, the concentration of oxygen vacancies decreased, resulting in reduced conductivity. This reduction in conductivity of $Zn_{0.9}Mg_{0.1}O$ NP ETL was confirmed through EOD characterization. It is noteworthy that the current density obtained from HOD fell within the range of the current densities obtained from EODs with thickness of 30 nm and 50 nm. Therefore, it is reasonable to conclude that charge balance in the QD EML is achieved in TE-QLED when using either a 30 nm or 50 nm thickness of $Zn_{0.9}Mg_{0.1}O$ as the ETL. Furthermore, the concentration of hydroxyl species was at its lowest in $Zn_{0.9}Mg_{0.1}O$ NP ETL with a thickness of 30 nm. The QLED with a 30-nm-thick $Zn_{0.9}Mg_{0.1}O$ NP ETL demonstrated the highest current efficiency and EQE. This can be attributed the fact that TE-QLED with the 30-nm-thick $Zn_{0.9}Mg_{0.1}O$ NP ETL had the lowest exciton quenching. As a result, the maximum current efficiency and maximum EQE of the TE-QLED reached 90.92 cd/A and 21.66%, respectively. These experimental results suggest that the use of the $Zn_{0.9}Mg_{0.1}O$ NP ETL layer with an appropriated thickness is a promising way to realize high-performance TE-QLEDs for next generation display and lighting applications.

Supplementary Materials: The following supporting information can be downloaded at preprints.org. Figure 1S Electroluminescence characteristics of QLEDs with a 50-nm-thick $Zn_{0.9}Mg_{0.1}O$ NP ETLs inside the bank enclosure and without bank: (a) Current density curves as a function of voltage, (b) Luminance curves as a function of voltage, (c) current efficiency curves as a function of current density, and electroluminescence spectra of the QLEDs utilizing $Zn_{0.9}Mg_{0.1}O$ NP ETLs

Author Contributions: G.-P.J. synthesized materials, fabricated and characterized the devices. H.-H.Y., S.-Y.K., Y.-B.C. performed the additional experiments and characterizations. H.-D.C. performed investigation. D.-G.M. conceptualized the work. C.K.K. conceptualized the work, wrote the manuscripts, performed project administration, resources, and supervision. All authors discussed the results and commented on the manuscript. All authors have read and agreed to the published version of the manuscript.

Funding: This research was partially supported by the Soonchunhyang University Research Fund and also supported by Korea Institute for Advancement of Technology (KIAT) grant funded by the Korea government (MOTIE) (P0012453, The Competency Development Program for Industry Specialist).

Data Availability Statement: The data that supports the findings of this study are available from the corresponding authors upon reasonable request.

Conflicts of Interest: The authors declare no conflict of interest. The funders had no role in the design of the study; in the collection, analyses, or interpretation of data; in the writing of the manuscript, or in the decision to publish the results.

References

1. Ekimov, A. I.; Hache, F.; Schanne-Klein, M. C.; Ricard, D.; Flytzanis, C.; Kudryavisev, I. A.; Yazeva, T. V.; Rodina, A. V.; Efros, A. I., Absorption and Intensity-Dependent Photoluminescence Measurement on CdSe Dots: Assignment of the First Electronic Transitions, *J. Opt. Soc. Am. B.* **1993**, 10, 100-107. https://doi.org/10.1364/JOSAB.10.000100
2. Efros, A. L.; Brus, L. E., Nanocrystal Quantum Dots: From Discovery to Modern Development, *ACS Nano*, **2021**, 15, 6192-6210. https://doi.org/10.1021/acsnano.1c01399
3. Shen, H.; Gao, Q.; Zhang, Y.; Lin, Y.; Lin, Q.; Li, Z.; Chen, L.; Zeng, Z.; Li, X.; Jia, Y.; Wang, S.; Du, Z.; Li, L. S.; Zhang, Z., Visible Quantum Dot Light-Emitting Diodes with Simultaneous High Brightness and Efficiency. *Nat. Photon*. **2019**, 13, 192–197. https://doi.org/10.1038/s41566-019-0364-z
4. Deng, Y.; Peng, F.; Lu, Y.; Zhu, X.; Jin, W.; Qiu, J.; Dong, J.; Hao, Y.; Di, D.; Gao, Y.; Sun, T.; Zhang, M.; Liu, F.; Wang, L.; Ying, L.; Huang, F.; Jin, Y., Solution-Processed Green and Blue Quantum-Dot Light-Emitting Diodes with Eliminated Charge Leakage, *Nat. Photonics*, **2022**, 16, 505–511. https://doi.org/10.1038/s41566-022-00999-9
5. Song, J.; Wang, O.; Shen, H.; Lin, Q.; Li, Z.; Wang, L.; Zhang, X.; Li, L. S., Over 30% External Quantum Efficiency Light–Emitting Diodes by Engineering Quantum Dot–Assisted Energy Level Match for Hole Transport Layer, *Adv. Funct. Mater*. **2019**, 29, 1808377. **https://doi.org/10.1002/adfm.201808377**
6. Mashford, B. S.; Stevenson, M.; Popovic, Z.; Hamilton, C.; Zhou, Z.; Breen, C.; Steckel, J.; Bulovic, B;, Bawendi, M., Coe-Sullivan, S., Kazlas, P. T., High-Efficiency Quantum-Dot Light-Emitting Devices with Enhanced Charge Injection, *Nat. Photon*. **2013**, 407-412. https://doi.org/10.1038/nphoton.2013.70
7. Moon, H.; Lee, C.; Lee, W.; Kim, J.; Chae, H., Stability of Quantum Dots, Quantum Dot Films, and Quantum Dot Light-Emitting Diodes for Display Applications, *Adv. Mater*. **2019**, *31*, 1804294. **https://doi.org/10.1002/adma.201804294**
8. Li, X.; Zhao, Y.-B.; Fan, F.; Levina, L.; Liu, M.; Quintero-Brmudez, R.; Gong, X.; Quan, L. N.; Fan, J. Z.; Yang, Z.; Hoogland, S.; Voznyy, O.; Lu, Z.-H.; Sargent, E. H.; Bright Colloidal Quantum Dot Light-Emitting Diodes Enabled by Efficient Chlorination, *Nat. Comm*. **2018**, 12, 159-164. https://doi.org/10.1038/s41566-018-0105-8
9. Qian, L.; Zheng, Y.; Xue, J.; Holloway, P. H. Stable and Efficient Quantum-Dot Light-Emitting Diodes Based on Solution-processed Multilayer Structures. *Nat. Photon*. **2011**, 5, 543–548. https://doi.org/10.1038/nphoton.2011.171
10. Su, Q.; Chen, S., Thermal Assisted Up-conversion Electroluminescence in Quantum Dot Light Emitting Diodes. *Nat. Commun*. **2022**, 13, No. 369. https://doi.org/10.1038/s41467-022-28037-w
11. Yang, Y.; Zheng, Y.; Cao, W.; Titov, A.; Hyvonen, J.; Manders, J. R.; Xue, J.; Holloway, P. H.; Qian, L. High-efficiency Light-Emitting Devices Based on Quantum Dots with Tailored Nanostructures. *Nat. Photon*. **2015**, 9, 259–266. https://doi.org/10.1038/nphoton.2015.36
12. Geffroy, B., le Roy, P., Prat, C., Organic Light-Emitting Diode (OLED) Technology: Materials, Devices and Display Technologies, *Polym. Int*. **2006**, 55, 572- 582. **https://doi.org/10.1002/pi.1974**

13. Thomschke, M.; Reineke, S.; Lüssem, B.; Leo, K. Highly Efficient White Top-Emitting Organic Light-Emitting Diodes Comprising Laminated Microlens Films. *Nano Lett*. **2012**, 12, 424 –428. https://doi.org/10.1021/nl203743p
14. Yang, J.-H.; Jang, G.-P.; Kim, S.-Y.; Chae, Y.-B.; Lee, K.-H.; Moon, D.-G.; Kim, C. K., Highly Efficient All-Solution-Processed Quantum Dot Light-Emitting Diodes Using MoOx Nanoparticle Hole Injection Layer, *Nanomaterials*, **2023**, 13, 2324. **https://doi.org/10.3390/nano13162324**
15. Lee, T.; Kim, B. J.; Lee, H.; Hahm, D.; Bae, W. K.; Lim, J.; Kwak, J. Bright and Stable Quantum Dot Light-Emitting Diodes. *Adv. Mater*. **2022**, 34, No. 2106276. **https://doi.org/10.1002/adma.202106276**
16. Lee, T.; Hahm, D.; Kim, K.; Bae, W. K.; Lee, C.; Kwak, J. Highly Efficient and Bright Inverted Top-Emitting Inp Quantum Dot Light-Emitting Diodes Introducing a Hole-Suppressing Interlayer, *Small*, **2019**, 15, No. 1905162. **https://doi.org/10.1002/smll.201905162**
17. Bae, W. K.; Brovelli, S.; Klimov, V. I., Spectroscopic Insights into the Performance of Quantum Dot Light-Emitting Diodes, *MRS Bull*. **2013**, 38, 721-730. https://doi.org/10.1557/mrs.2013.182
18. Sun, Y.; Jiang, Y.; Peng, H.; Wei, J.; Zhang, S.; Chen, S., Efficient Quantum Dot Light-Emitting Diodes with a Zn0.85Mg0.95O Interfacial Modification Layer, *Nanoscale*, **2017**, 9, 8962-8969. **https://doi.org/10.1039/C7NR02099F**
19. Heo, S. B.; Shin, J. S.; Kim, T. Y.; Park, S.; Jung, W. H.; Kim, H.; Hong, J.-A.; Kim, B.-S.; Park, Y.; Chin, B. D.; Kim, J.-G.; Kang, S. J., Highly Efficient and Low Turn-on Voltage Quantum-Dot Ligh-Emitting Diodes Using a ZnMgO/ZnO Double Electron Transport Layer, *Curr. Appl. Phys*. **2021**, 29, 107-113. https://doi.org/10.1016/j.cap.2021.07.001
20. Qasim, K.; Chen, J.; Xu, F.; Wu, J.; Li, Z.; Lei, W.; Cui, Y.; Xia, J., Large Area Quantum-Dot Light Emitting Diode Arrays with ZnO Nanoparticles as Electron Transport/Injection Layer, *Sci. Adv. Mater*. **2014**, 6, 2625-2531. https://doi.org/10.1166/sam.2014.2013
21. Bae, W. K.; Park, Y.-S.; Lim, J.; Lee, D.; Padilha, L. A.; McDaniel, H.; Robel, I.; Lee, C.; Pietryga, J. M.; Klimov, V. I., Controlling the Influence of Auger Recombination on the Performance of Quantum-Dot Light-Emitting Diodes, *Nat. Comm*. **2013**, 4, 2661. https://doi.org/10.1038/ncomms3661
22. Dai, X., Zhang, Z, Jin, Y., Niu, H., Cao, H., Liang, X., Chen, L., Wang, J., Peng, X., Solution-Processed, High-Performance Light-Emitting Diodes Based on Quantum Dots, *Nature*, **2014**, 515, 96-99. https://doi.org/10.1038/nature13829
23. Zhang, Z; Ye, Y.; Pu, G.; Deng, X.; Dai, X.; Chen, X.; Chen, D.; Zheng, X.; Gao, Y.; Fang, W.; Peng, X.; Jin, Y., High-Performance, Solution-Processed, and Insulating-Layer-Free Light-Emitting Diodes, Based on Colloidal Quantum Dots, *Adv. Mater*. **2018**, 30, 1801387. **https://doi.org/10.1002/adma.201801387**
24. Wu, H.; Zhang, Y.; Zhang, M.; Lu, M.; Sun, C.; Zhang, T.; Yu, W. W., Enhanced Stability and Performance in Perovskite Nanocrystal Light-Emitting Devices Using a ZnMgO Interfacial Layer, *Adv. Opt. Mater*. **2017**, 5, 1700377. **https://doi.org/10.1002/adom.201700377**
25. Wang, L.; Liu, J.; Liu, X.; Cao, S.; Wang, Y.; Zhao, J.; Zou, B., Mg-Doped ZnO Nanoparticle Film as the Interlayer between the ZnO Electron Transport Layer and Quantum Dot Layer for Light-Emitting Diodes, *J. Phys. Chem*. **2020**, 124, 8758-8765. https://doi.org/10.1021/acs.jpcc.0c00351
26. Qu, X.; Liu, W.; Li, D.; Ma, J.; Gu, M.; Jia, S.; Xiang, G.; Sun, X. W., Does Interfacial Exciton Quenching Exist in High-Performance Quantum Dot Light-Emitting Diodes, *Nanoscale*, **2023**, 15, 3430-3437. **https://doi.org/10.1039/D2NR07119C**
27. Chrzanowski, M.; Kuchowicz, M.; Szukiewicz, R.; Sitarek, P.; Misiewicz, J., Enhancing Efficiency of Quantum Dot Light-Emitting Diode by Sol-Gel Derived Zn1-xMgxO Electron Transport Layer, *Org. Electron*. **2020**, 80, 105656. https://doi.org/10.1016/j.orgel.2020.105656
28. Moon, H.; Lee, W.; Kim, J.; Lee, D.; Lee, D.; Cha, S.; Shin, S.; Chae, H., Composition-Tailored ZnMgO Nanoparticles for Electron Transport Layers of Highly Efficient and Bright InP-Based Quantum Dot Light Emitting Diodes, *Chem. Comm*. **2019**, 55, 13299-13302. **https://doi.org/10.1039/C9CC06882A**
29. Kim, J.-H.; Han, C.-Y.; Lee, K.-H.; An, K.-S.; Song, W.; Kim, J.; Oh, M. S.; Do, Y. R.; Yang, H., Performance Improvement of Quantum Dot-Light-Emitting Diodes Enabled by an Alloyed ZnMgO Nanoparticle Electron Transport Layer, *Chem. Mater*. **2015**, 27, 197-204. https://doi.org/10.1021/cm503756q
30. Eun, Y.-B.; Jang, G.-P.; Yang, J.-H.; Kim, S.-Y.; Chae, Y.-B.; Ha, M.-Y.; Moon, D.-G.; Kim, C.-K., Performance Improvement of Quantum Dot Light-Emitting Diodes Using a ZnMgO Eectron Transport Layer with a Core/Shell Structure, *Materials*, **2023**, 16, 600. **https://doi.org/10.3390/ma16020600**
31. Ning, M.; Zhao, K.; Zhao, L.; Cao, S.; Zhao, J.; Gao, Y.; Yuan, X., Passivating Defects in ZnO Electron Transport Layer for Enhancing Performance of Red InP-Based Quantum Dot Light-Emitting Diodes, Mater. Res. Bull. to be published. https://doi.org/10.1016/j.materresbull.2023.112589
32. Liu, D.; Cao, S.; Wang, S.; Wang, H.; Dai, W.; Zou, B.; Zhao, J.; Wang, Y., Highly Stable Red Quantum Dot Light-Emitting Diodes with Long T95 Operation Lifetimes, *J. Phys. Chem. Lett*. **2020**, 11, 3111-3115. https://doi.org/10.1021/acs.jpclett.0c00836
33. Hsieh, Y. C.; Chen, P. T.; Kao, K. S.; Wang, C. M, Luminescence Mechanism of ZnO Thin Film Investigated by XPS Measurement, *Appl. Phys. A*, **2008**, 90, 317-321. https://doi.org/10.1007/s00339-007-4275-3

34. Rim, Y.S.; Kim, D.L.; Jeong, W.H.; Kim, H.J., Effect of Zr Addition on ZnSnO Thin-Film Transistors Using a Solution Process, *Appl. Phys. Lett*. **2010**, 97, 233502. https://doi.org/10.1063/1.3524514
35. Zheng, Z.H.; Jiang, Q.; Lian, J. S., Synthesis and Optical Properties of Flower-Like ZnO Nanorods by Thermal Evaporation Method, *Appl. Surf. Sci*. **2011**, 257, 5083. https://doi.org/10.1016/j.apsusc.2011.01.025
36. Han, X. G.; He, H. Z.; Kuang, Q.; Zhou, X.; Zhang, X.H.; Xu, T.; Xie, Z.X,; Zheng, L.S., Controlling Morphologies and Tuning the Related Properties of Nano/Microstructured ZnO Crystallites, *J. Phys. Chem*. **2009**, 113, 584. https://doi.org/10.1021/jp808233e.
37. Y. H. Wang, Q. Ma, L. L. Zheng, W. J. Liu, S. J. Ding, H. L. Lu, D. W. Zhang, Performance Improvement of Atomic Layer-Deposited ZnO/Al_2O_3 Thin-Film Transistors by Low-Temperature Annealing in Air, *IEEE Trans. Electron Devices*, **2016**, 63, 1893-1898. 10.1109/TED.2016.2540679
38. Liu, S.; Ho, S.; Chen, Y.; So, F., Passivation of Metal Oxide Surfaces for High-Performance Organic and Hybrid Optoelectronic Devices, *Chem. Mater*. **2015**, 27, 2532-2539. https://doi.org/10.1021/acs.chemmater.5b00129
39. Wood, V.; Panzer, M.; Caruge, J.; Halpert, J.; Bawendi, M.; Bulovic, V., Air-Stable Operation of Transparent, Colloidal Quantum Dot Based LEDs with a Unipolar Device Architecture, *Nano Lett.* **2010**, 10, 24-29. https://doi.org/10.1021/nl902425g
40. Veijo, J.; Jensen, K.; Mattoussi, H.; Michel, J.; Dabbousi, B.; Bawendi, M., Cathodoluminescence and Photoluminescence of Highly Luminescence CdSe/ZnS Quantum Dot Composite, *Appl. Phys. Lett.* **1997**, 70, 2132-2134. https://doi.org/10.1063/1.119043
    Empedocles, S.; Bawendi, M., Quantum-Confined Stark Effect in Single CdSe Nanocrystallite Quantum Dots, *Science*, **1997**, 278, 2114-2117. https://doi.org/10.1126/science.278.5346.2114